The Journal of Experimental Biology 199, 2611–2618 (1996)
Printed in Great Britain © The Company of Biologists Limited 1996
JEB0284

SIZE-DEPENDENCE OF WATER-RUNNING ABILITY IN BASILISK LIZARDS (*BASILISCUS BASILISCUS*)

J. W. GLASHEEN[1,*] AND T. A. MCMAHON[2]

[1]*Department of Organismic and Evolutionary Biology* and [2]*Division of Applied Sciences, Harvard University, Cambridge, MA 02138, USA*

Accepted 14 August 1996

Summary

In the past, it has been proposed that basilisk lizards (*Basiliscus basiliscus*) are able to reach high population densities because the juveniles and adults have differing water-running abilities and therefore live in different habitats. However, there is no *a priori* reason to expect juveniles to be better able to run on water than adults. To determine the causal relationship between body size and water-running ability, we made three types of measurements: (1) direct morphological measurements on preserved specimens; (2) hydrodynamic measurements on physical models of the lizards' feet; and (3) kinematic measurements on basilisk lizards running on water. The information gathered from these investigations was used to develop an allometric model which predicted the maximum upward force impulses that the lizards could generate. We find that small lizards have a capacity to generate large force surpluses. A 2 g lizard can generate a maximum upward impulse that is more than twice that needed to support its body weight (225 %). In contrast, a 200 g lizard, under optimal conditions, can just barely support its body weight (111 %).

Key words: basilisk lizard, allometry, locomotion, fluid dynamics, air–water interface, unsteady flow, biomechanics, running on water.

Introduction

The apparently size-dependent ability of basilisk lizards (*Basiliscus basiliscus*) to run on water is thought to play a crucial role in their population dynamics (Laerm, 1974). Juvenile basilisk lizards are able to run across the water surface with ease. They can even start under water, accelerate their center of mass upwards, and be above the water surface in just a few steps. In contrast, adult basilisks appear to struggle to run on the water surface (Rand and Marx, 1967) and their running often degenerates into swimming. The apparent variation in ability to run on water may cause juveniles and adults to live in different habitats. This might lead to resource partitioning, which could be responsible for the ability of basilisks to reach very high population densities (Laerm, 1974; van Devender, 1983). However, without a fundamental physical understanding of the dependence of water-running ability on body size, any claim of causal relationships among water-running ability, habitat preference and body size is only conjecture.

Previously, to develop such a physical understanding, we investigated the forces that are produced when a flat disk enters the water, taking care to approximate the size and speed of the disks to those of the lizards' feet (Glasheen and McMahon, 1996*a*). Three fundamental phenomena were found to be of particular importance in low-speed water entry: (1) impact; (2) air-cavity formation; and (3) cavity seal. When an object strikes the water surface, a volume of water near the object is accelerated suddenly downwards. As the object continues downwards, fluid particles beneath the object are displaced laterally while an air cavity forms above. Finally, hydrostatic pressure accelerates fluid particles radially inwards, so that eventually the cavity is sealed off from the atmospheric air. In a related study, the results of low-speed water-entry experiments were used to develop a simple hydrodynamic model for moderately sized basilisks (approximately 90 g) running on water (Glasheen and McMahon, 1996*b*). The model was able to predict not only the forces that are produced when a lizard's foot slaps and strokes into the water but also how quickly the lizard must pull its foot out of the water in order to avoid cavity collapse.

In this investigation, we incorporate morphological, hydrodynamic and kinematic data in an allometric model which probes the effect of body size on water-running ability. In particular, we ask the question: is there a physical basis for the ontogenetic variation in water-running performance?

Materials and methods

Morphological measurements

Forty-two preserved specimens (*Basiliscus basiliscus*;

*Present address: McKinsey and Company, Inc., Two Crossroads Drive, Bedminster, NJ 07921, USA (e-mail: james_glasheen@mcKinsey.com).

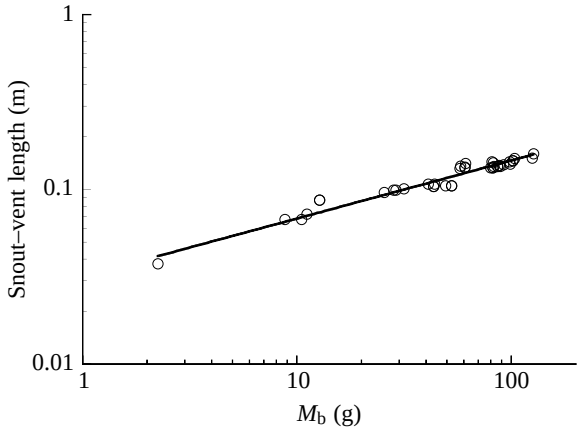

Fig. 1. Gross morphological measurements made on live *Basiliscus basiliscus* lizards. The relationship between snout–vent length (*SVL* in m) and body mass (M_b in g) of live lizards was then used to estimate the live body masses of museum specimens ($SVL=0.0317M_b^{0.332}$, $r=0.972$, $P_{slope}<0.0001$, $P_{y\text{-}int}<0.0001$; 41 measurements).

Museum of Comparative Zoology, Harvard University, USA) were used to obtain allometric relationships among foot length (L_F), leg length (L_L) and snout–vent length (*SVL*). *SVL* was defined as the distance from the tip of the snout to the posterior edge of the anterior lip of the vent. L_F is the distance between the heel and the tip of the fourth toe. L_L is the distance from the proximal articulation of the leg to the heel. However, the live body masses (M_b) of the preserved specimens were unknown. Thus, it was necessary to establish a relationship between *SVL* (in m) and M_b (in g) of the live lizards (for which only gross morphological measurements, such as *SVL*, were available) used in our kinematic experiments (Fig. 1). Using this relationship, it was possible to estimate the live M_b for the preserved specimens. Power curves were fitted to graphs which related L_F and L_L to M_b.

Ten preserved specimens which had measurements that lay close to the power-curve fit relating L_F to M_b were selected for detailed measurements of their feet. Vernier calipers were used for all measurements. The expanded-toe width was measured by placing a toe on a flat horizontal surface and lightly compressing it from above while simultaneously extending the lateral toe fringe. Measurements of the distance from the heel to the metacarpal–phalangeal joint (MP) and from the MP to the tip of the toe were also obtained for each toe. Finally, the width of the plantar surface at the level of the MP of the first toe was measured.

The detailed measurements of the feet were used to construct physical models out of aluminum sheet metal (thickness 0.762 mm). Model foot area was calculated by weighing each model and comparing the mass with that of a standard of known area. To minimize model foot vibrations, a small piece of vertically oriented aluminum sheet metal formed a buttress on the upper side of each toe of every foot. The buttresses did not affect fluid flow, as video records showed that they were wholly contained in the air cavity throughout the entire period of force measurement.

Missile experiments

Each of the ten model feet was attached using petrowax to an apparatus designed to measure the forces produced during low-speed water entry (Fig. 2A). By varying the point of attachment of the foot model slightly until a missile-drop experiment resulted in little or no tilting of the missile apparatus during the entire period of force measurement, we ensured that the foot model's center of pressure was aligned

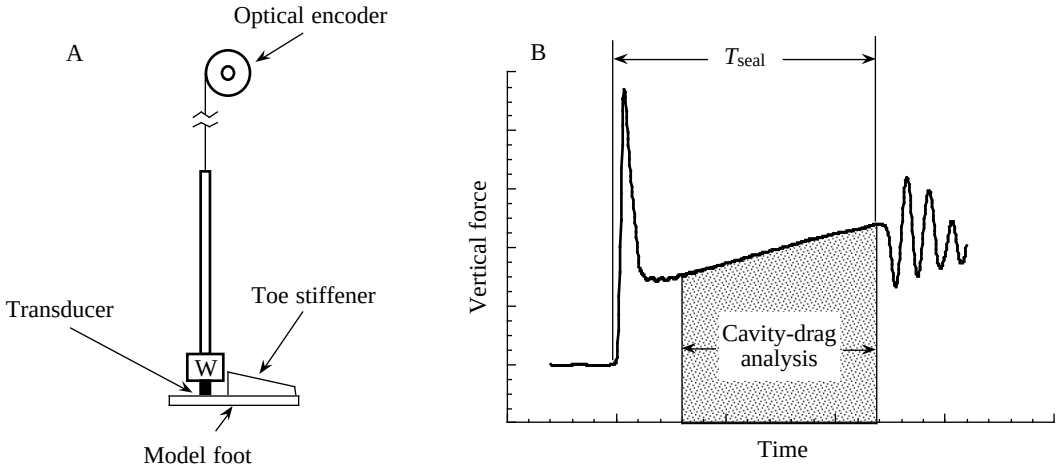

Fig. 2. (A) The missile apparatus. A foot model was attached directly to a transducer, which was connected to a weight (W) and a long rod. In impact experiments, the transducer was an accelerometer, while in cavity-drag experiments a force transducer was used. The missile was connected *via* fishing line to a pulley mounted on a rotary optical encoder. (B) A diagrammatic force record. When a foot model drops into water, a transient, high-amplitude force impulse is generated as water in the vicinity of the foot model is accelerated from rest to the foot model's speed. Following impact, an air cavity, which extends up from the foot model and is open to atmospheric air, is expanded by the downward movement of the foot model. Drag forces rise during this period due to increasing pressure differences between atmospheric pressure in the air cavity and the hydrostatic pressure encountered by the foot model. Finally, the air cavity seals below the water surface, resulting in high-amplitude force oscillations. Cavity-drag analysis begins only after impact forces have been dissipated and ends immediately before the cavity seals. T_{seal} is the period between impact and cavity closure.

with the central axis of the missile. The missile apparatus consisted of a transducer attached to a weight and a long rod. In one set of experiments, designed to measure the force impulse produced during the initial impact with the water surface, the foot model was attached directly to an accelerometer (model 8630B50, Kistler Instrument Corp., Amherst, NY, USA). A light, flexible cable (nylon monofilament fishing line) attached to the top of the long rod ran over a light pulley, so that an optical encoder (model H1-512-E, U.S. Digital Corp., Vancouver, WA, USA) on the pulley shaft gave a measurement of the downward velocity of the model just before impact (Fig. 2A). For each foot model, a linear fit was applied to measurements relating the slap impulse of the foot model to the impact speed (0.605–2.46 m s^{-1}; 40 measurements per foot model). With a knowledge of the density of water (ρ), it is possible to calculate the radius of a disk (r_{eff}) that would generate the same relationship between the slap impulse of a foot model and impact speed, u_{impact}, (Glasheen and McMahon, 1996*a*; Birkhoff and Zarantonello, 1957):

$$r_{eff} = \{\text{foot model slap impulse}/[(4/3)\rho u_{impact}]\}^{0.33}. \quad (1)$$

In experiments designed to measure the drag force as the foot model continued downwards after the impact, the accelerometer was replaced by a force transducer (model ELF-TC500-20, Entran Devices, Fairfield, NJ, USA). Following the force peak associated with impact, the drag force rose as the foot model descended at a nearly constant velocity (the change in model-foot velocity was less than 5% of the root-mean squared velocity of the foot model; Fig. 2B). A high-speed video camera (NAC, HSV-200, Tokyo, Japan; 500 fields s^{-1}) recorded the depth of the foot model during the continuing downward stroke after impact. During this time (the cavity-drag phase), an air-filled cavity extended from the foot model to the surface. The drag was measured up to the moment at which the cavity collapsed and was sealed off from the atmospheric air. A water-entry drag coefficient (C_D^*) was defined as:

$$C_D^* = D(t)/[0.5S\rho u^2 + S\rho \boldsymbol{g} h(t)], \quad (2)$$

where $D(t)$ is the time-varying drag, S is the foot area, u is the velocity, $\boldsymbol{g}$ is the gravitational acceleration, and $h(t)$ is the time-varying depth of the foot model below the water surface. For a flat, circular disk, C_D^* has been shown to be constant, regardless of size, speed or cavity depth within the parameter ranges appropriate for basilisk water-running (Glasheen and McMahon, 1996*a*). In the present experiments, C_D^* had a (slightly) different constant value for each foot. T_{seal} was obtained by measuring the period between impact and cavity closure (Fig. 2B). Further details regarding measurement of the impact and drag forces as well as the timing of cavity collapse are explained in Glasheen and McMahon (1996*a*). A method for estimating the relative force contribution of surface tension is presented in Appendix A.

Kinematic measurements

Ten basilisk lizards (*Basiliscus basiliscus*) were captured in Golfito, Costa Rica, and brought to Cambridge, MA, USA (M_b 2.25–127.2 g). All animals were housed and cared for following procedures established by the Committee for the Use of Animals in Teaching and Research of the Faculty of Arts and Sciences, Harvard University, USA. In each trial, a single lizard was placed in an enclosure that was elevated slightly above the surface of a large tank of water (3.66 m long by 0.43 m wide by 0.30 m deep). To stimulate the lizard to run across the water surface, one side of the enclosure was opened suddenly while simultaneously startling the lizard from the opposite side by a clap of the hands. The lizard's motions were recorded in a side view using high-speed video at 500 fields s^{-1} (HSV-1000, Eastman Kodak Company, Northboro, MA, USA). Analysis of sequences in which the lizard maintained a constant height above the water surface yielded measurements of the stride frequency (f_{str}) and the position of the foot *vs.* time. The downward velocity of the mid-foot [$u(t)$] was calculated by measuring the displacement of the mid-foot [$h(t)$], fitting a seventh-order polynomial, and evaluating the derivative of the polynomial. Peak velocity (u_{peak}) and root-mean-square velocity (u_{rms}) were obtained from an analysis of $u(t)$. Body mass was recorded immediately after each experiment.

Model development

We developed a hydrodynamic model which uses results from our previous study of the dynamics of flat, circular disks entering the water (Glasheen and McMahon, 1996*a*) to predict several observable measures of how lizards of different body sizes run on water. The model consists of three phases: (1) slap; (2) stroke; and (3) protraction. The maximum slap impulse that a lizard could produce was estimated using the equation:

$$\text{maximum slap impulse} = (4/3)\rho r_{eff}^3 u_{peak}. \quad (3)$$

The allometry of the effective disk radius, r_{eff}, was determined from the hydrodynamic experiments using the 10 model feet. Analysis of the video records showed that the peak downward velocity u_{peak} was extremely variable, even for a single lizard, and was not a regular function of body size. To fix the parameters of our model, a value of 3.75 m s^{-1} was taken as a reasonable upper bound for u_{peak} in lizards of all body sizes. Once r_{eff} had been determined for a lizard of a given body size, the maximum possible slap impulse was calculated using equation 3, taking the upper-bound value of 3.75 m s^{-1} for u_{peak}. In addition to calculating the maximum possible slap impulse, we also calculated the slap impulse for a given step by using the actual u_{peak} measured for that step.

A model for the maximum stroke impulse was also developed. The model assumes a vertical downward stroke at a constant velocity (u_{rms}) to a depth equal to that of the lizard's leg (L_L), while keeping the foot orthogonal to the direction of travel throughout the entire stroke. The stroke impulse may be defined as the product of the average drag force and the time over which the drag force is applied:

$$\text{maximum stroke impulse} = (0.5C_D^* S\rho u_{rms}^2 + 0.5C_D^* S\rho \boldsymbol{g} L_L)(L_L/u_{rms}). \quad (4)$$

The total drag force is due to two sources of a pressure differential across the foot. First, there is a constant drag due to the inertia of the fluid ($0.5C_D^*S\rho u_{rms}^2$). Second, as depth increases, the pressure difference between the hydrostatic pressure at a particular level in the water and the atmospheric pressure in the air cavity increases. Thus, the average drag due to hydrostatic pressure is $0.5C_D^*S\rho \boldsymbol{g} L_L$. The time over which the stroke force is applied is L_L/u_{rms}. To obtain a general model for how the stroke impulse varies with size, allometric relationships were substituted for C_D^*, S and L_L. Kinematic analysis of the video images provided an estimate of the greatest value for u_{rms} in all runs of all animals ($2.5\,m\,s^{-1}$). Estimates of maximum stroke impulse contributions obtained using equation 4 with parameters determined as explained above agree well with detailed measurements in which the variation of foot angle and foot speed are taken into account (see Appendix B).

Finally, in addition to estimating the upper bounds for the maximum slap and stroke impulses, we developed a model which predicts the upward impulse needed to maintain the center of mass at a constant height. We assume that downward drag forces produced during foot protraction are negligible, because our video records show that the lizard protracts its foot within the air cavity. Protraction drag is further minimized by the feathering of the lateral toe fringes and the plantar flexion of the foot such that the foot's long axis is parallel to the direction of travel. Thus, the minimum needed impulse is simply the product of the body weight and the period between steps (T_{step}):

$$\text{minimum needed impulse} = M_b \boldsymbol{g} T_{step}. \quad (5)$$

Analysis of the video records showed that stride frequencies between 5 and 10 Hz were used by all animals, with no clear dependence on body mass. Therefore, for the model calculations, we assumed an upper bound of 10 Hz on f_{str}, independent of M_b. Since the video records show that there is rarely a time within a stride when either two feet or no feet are in the water, we assumed that the minimum T_{step} is 0.05 s ($T_{step}=0.5f_{str}^{-1}$). In addition to calculating the minimum needed impulse, we also calculated the actual needed impulse for a given step by using the measured step period for that sequence.

Results

Simple measurements of the lizards' gross morphology indicate that they grow isometrically (a characteristic length is proportional to $M_b^{0.33}$). Leg length (in m) scaled close to isometry [$L_L=0.0165M_b^{0.338}$, r=0.986] over an almost 100-fold range in body mass (2.03–179 g; Fig. 3A), as did foot length ($L_F=0.0164M_b^{0.302}$, r=0.990; Fig. 3B). However, mass measurements of the aluminum model feet (Fig. 4) showed that foot area (S, in m^2) scaled with negative allometry, since the exponent of M_b for an area measurement was less than 0.67 ($S=5.39\times10^{-5}\ M_b^{0.538}$, r=0.998, $P_{slope}<0.0001$, $P_{y\text{-}int}=0.0002$). In the above allometric formulae and throughout, M_b is specified in grams. Also, the P_{slope} and $P_{y\text{-}int}$ of a given power-fit reflect the respective significance of a slope and y-intercept (y-int) greater than 0.

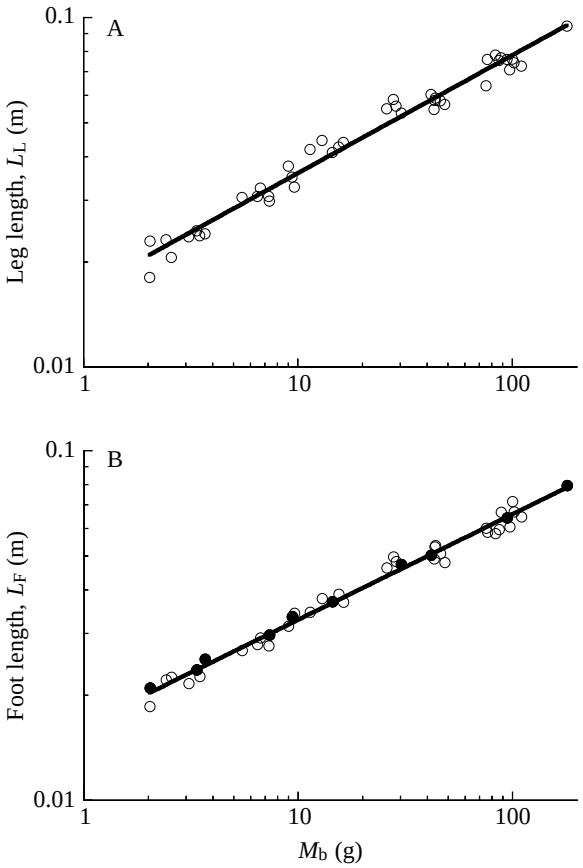

Fig. 3. Morphological allometry. All measurements are from museum specimens. (A) The distance from the hip to the heel, leg length (L_L), and (B) from the heel to the tip of the fourth toe, foot length (L_F), increase isometrically over nearly two orders of magnitude in body mass ($L_L=0.0165M_b^{0.338}$, r=0.986, $P_{slope}<0.0001$, $P_{y\text{-}int}<0.0001$; $L_F=0.0164M_b^{0.302}$, r=0.990, $P_{slope}<0.0001$, $P_{y\text{-}int}<0.0001$). The filled symbols in B represent specimens that were selected for detailed foot measurements.

Measurements made during the missile-drop experiments using the model feet complemented those made directly on the morphology of the museum specimens. The effective radius, r_{eff} (in m), a quantity that incorporates changes in shape as well as size, scaled with negative allometry ($r_{eff}=4.37\times10^{-3}M_b^{0.252}$, r=0.995; Fig. 5). By combining the results for r_{eff} with information from missile-drop experiments using disks (Glasheen and McMahon, 1996*a*), it was possible to generate predictions for both the timing of cavity collapse and the drag force. Consider, first, the drag force during the cavity-drag period (see Fig. 2B). For a given depth and downward velocity, the drag is proportional to the product of C_D^* and S (equation 2). The missile-drop experiments using the model feet showed that C_D^* remained nearly constant over the entire range of body size ($C_D^*=0.724M_b^{-0.021}$, r=0.532, P_{slope}=0.0933, $P_{y\text{-}int}<0.0001$). Thus, when C_D^*S is plotted against M_b (Fig. 6), the increase in the product C_D^*S with increasing body size is due almost entirely to the growth of foot area. In Fig. 6, foot area S was determined by weighing each foot model cut from

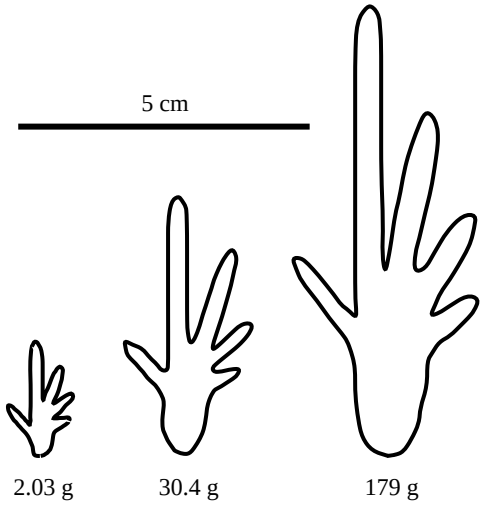

Fig. 4. Tracings of three of the ten foot models. Detailed foot measurements were used to construct physical models of the lizards' feet. Impact and drag forces as well as the timing of air-cavity collapse were measured in hydrodynamic experiments using these foot models. Although the shape of each foot model is quite different from that of a disk, calculations based on measurements from disks were able to predict many of the results from hydrodynamic experiments using the foot models (Glasheen and McMahon, 1996*a*).

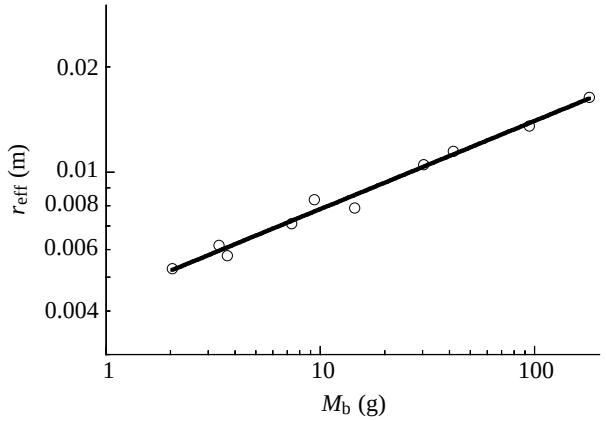

Fig. 5. Impact allometry. Measurements obtained from physical models of the lizards' feet. The effective radius (r_{eff}) of a lizard's foot increases less rapidly than L_L or L_F as body mass increases ($r_{eff}=4.37\times10^{-3}M_b^{0.252}$; r=0.995, P_{slope}<0.0001, $P_{y\text{-}int}$<0.0001). r_{eff} is defined as the radius of a disk that would generate the same relationship between slap impulse and impact speed as that of the foot model.

aluminum sheet (see Fig. 4), and C_D^* was obtained for each foot model using equation 2 and measurements of $D(t)$, $h(t)$ and u from 20 missile-drop experiments per foot model. In a test of the hypothesis that the relationships among the slap impulse, the cavity drag and the timing of cavity closure are insensitive to changes in the shape of a two-dimensional object striking flat on the water, a completely separate set of measurements, the impact experiments (Fig. 5), was used to determine an allometric equation for the equivalent disk area

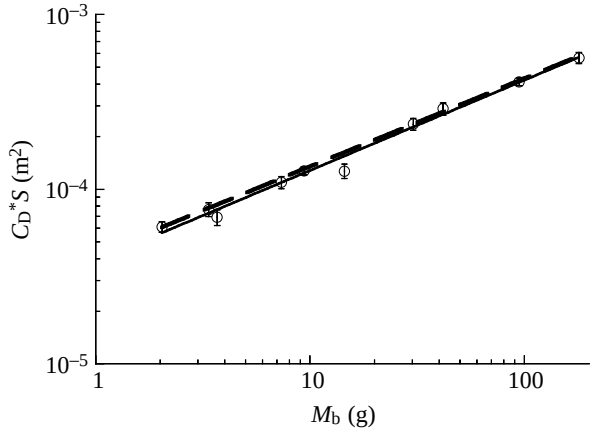

Fig. 6. Cavity-drag allometry. For a given speed and depth, the product of the water-entry drag coefficient (C_D^*) and the foot area (S) determines the drag forces during the cavity-drag period for the foot model experiments that produced these results. C_D^* values were determined from equation 2 using measurements of $D(t)$ from the force transducer (Fig. 2B) and measurements of u from the polynomial fits to data from video images showing the vertical position of a foot model *versus* time; foot area S was determined by weighing the aluminum-sheet foot models. The points (means ± S.D., 20 measurements for each foot model) are compared with a calculated line which is based on the drag coefficient of a disk and the effective foot area calculated from the impact experiments [broken bold line; $C_D^*(\text{disk})S_{eff}=0.703\pi r_{eff}^2$; where $r_{eff}=4.37\times10^{-3}M_b^{0.252}$]. The solid line is a power fit to the mean C_D^*S data.

of a foot model ($S_{eff}=\pi r_{eff}^2=6.00\times10^{-5}M_b^{0.504}$). The product of S_{eff} and the C_D^* of a disk (where $C_D^*=0.703$; Glasheen and McMahon, 1996*a*) generates a prediction of how C_D^*S would depend on M_b if the relationship between the slap impulse and cavity drag is the same whether measurements are made with disks or with model feet (Fig. 6; predicted C_D^*S = broken bold line = $4.22\times10^{-5}M_b^{0.504}$). The agreement between the measurements and the prediction is quite close (Fig. 6; fit of C_D^*S = solid light line = $3.88\times10^{-5}M_b^{0.517}$; r=0.997, P_{slope}<0.0001, $P_{y\text{-}int}$<0.0006).

The information derived from impact experiments can also be used to predict how T_{seal}, the period between impact and cavity closure, varies with body size. First, measurements of the timing of cavity closure were obtained from force records collected during cavity-drag experiments with the model feet (Fig. 2B). Each foot model generated a cavity which sealed after a characteristic time (T_{seal}). On the basis of measurements from all the model feet, a plot of the allometry of T_{seal} was obtained (Fig. 7). The direct measurements were compared with a theory developed from experiments conducted with disks. For disks, there is a relationship between the timing of cavity closure and disk radius. If this relationship is the same regardless of whether the object is a disk or a foot model, then the measurements should fall along this line (Fig. 7; predicted T_{seal} = broken bold line = $0.0483M_b^{0.126}$; fit of T_{seal} = solid light line = $0.0473M_b^{0.132}$; r=0.994, P_{slope}=0.0009, $P_{y\text{-}int}$<0.0001).

In contrast to morphological and hydrodynamic

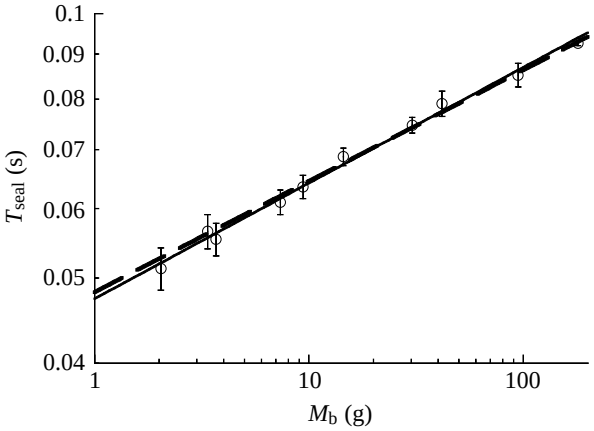

Fig. 7. Cavity-seal allometry. Larger foot models create cavities which remain open for longer than do the cavities created by the smaller foot models. The period between impact and cavity closure (T_{seal}) is shown (mean ± S.D.; N=20). The results are compared with a calculated curve (broken line) based on the r_{eff} derived from the impact experiments and the results from cavity closure experiments with disks [broken bold line; $T_{seal}=2.285(r_{eff}/\boldsymbol{g})^{0.5}$; where $\boldsymbol{g}$ is gravitational acceleration and $r_{eff}=4.37\times10^{-3}M_b^{0.252}$]. The solid light line is a power fit to the mean T_{seal} data.

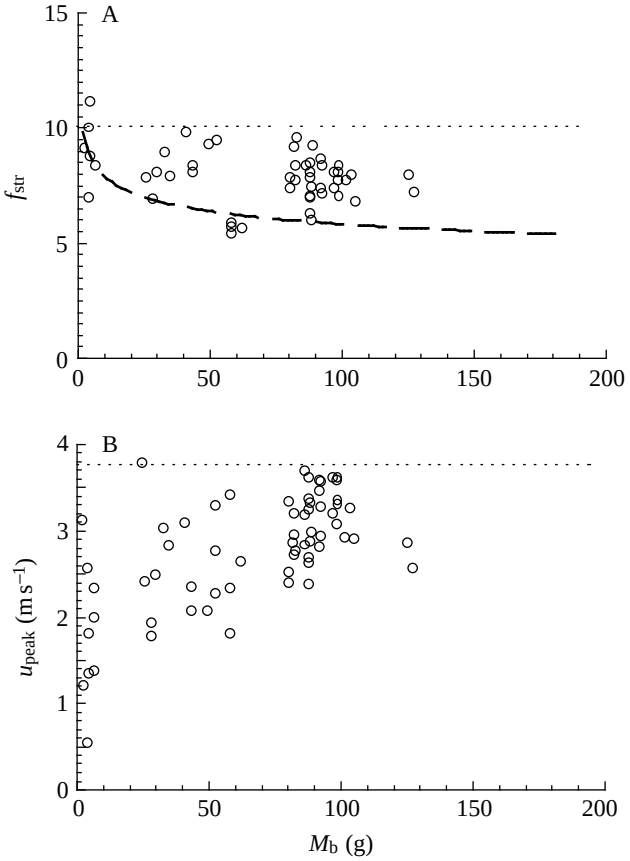

Fig. 8. Kinematic allometry. Stride frequency, f_{str}, is measured as the inverse of the period between water strikes of the same foot of lizards running in a large tank. (A) Larger lizards tended to use a f_{str} that is above a theoretical minimum (dashed curve). The minimum f_{str} is defined as the lowest stride frequency which would still allow a lizard to pull its foot out of the water before the air cavity collapses. The assumed maximum stride frequency used in the hydrodynamic model is also shown (dotted line). (B) The peak downward velocity of the midpoint of the foot (u_{peak}) is extremely variable. The assumed maximum u_{peak} used in the hydrodynamic model is also shown (dotted line).

measurements, the kinematics of the lizards running on water did not show a strong trend with increasing body size. Lizards of all body sizes use stride frequencies ranging from 5 to 10 Hz (Fig. 8A). However, all but the smallest lizards seem to be constrained to run at a f_{str} that is greater than a theoretical minimum. A prediction of the minimum stride frequency ($f_{str,min}$, in Hz) was generated on the basis of measurements of the timing of cavity seal by assuming that, at the moment of cavity seal, the foot that created the cavity is above the depth at which the cavity seals. Simultaneously, the other foot is just beginning the slap phase [$f_{str,min}=(2T_{seal})^{-1}=10.35M_b^{-0.126}$; Fig. 8A]. Measurements of the peak velocity of the mid-foot, u_{peak}, also show great variability for lizards of all sizes (Fig. 8B). Estimates of the upper limit of u_{peak} (3.75 m s^{-1}) and u_{rms} (2.5 m s^{-1}) for lizards of all sizes were used in calculations of the maximum slap and stroke impulses, respectively.

An allometric model which combines morphological, hydrodynamic and kinematic data generated predictions which agree well with calculations of the slap-impulse contribution from lizards over a range in sizes (Fig. 9). On the basis of calculations of the maximum contributions from slap and stroke impulses [(maximum slap impulse/minimum needed impulse) × 100 = $84.8M_b^{-0.244}$; (maximum stroke impulse/minimum needed impulse) × 100 = $177M_b^{-0.158}+4.17M_b^{0.180}$], the model can predict what range of impulses is possible for lizards of a given size. For example, the model predicts that a 200 g lizard is constrained to a relatively narrow range of contributions from the slap impulse (12.3–23.3 % of the overall needed force impulse in a step). In contrast, a 2 g lizard can vary its use of the slap impulse to a large degree (0–71.7 %).

Discussion

Rand and Marx (1967) observed that basilisk lizards over a broad size range are able to run on the water surface and support their body weight. However, they noted that adults failed in their attempts to run on the water surface much more frequently than did juveniles. The results of the present study indicate that there is a physical basis for their observations. First, our model suggests that lizards ranging in size from 2 to 200 g have the capacity to generate more than enough force to support their body weight. In fact, small lizards can support their body weight by generating a large slap impulse and a small stroke impulse, or a small slap impulse and a large stroke impulse, or intermediate values of both impulses. However, as lizards grow larger, they are constrained to use an increasingly narrow range of possible slap and stroke impulse combinations. This narrowing range of impulse combinations

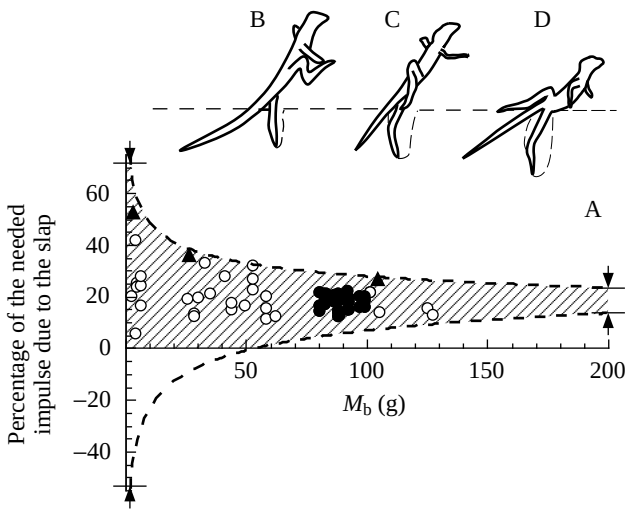

Fig. 9. The relative contribution of the slap impulse. (A) The percentage of the needed impulse that is generated by the slap impulse varies with body mass. Small lizards display a large range in the degree to which they can use the slap impulse. In contrast, large lizards are constrained to use a relatively small range of slap impulses. The hatched area shows the range of possible slap-impulse contributions for steady locomotion. The vertical distance between the maximum (upper dashed curve) and minimum (lower dashed curve) slap-impulse contribution curves for a lizard of a given body mass (M_b) illustrates the maximum relative impulse surplus (maximum impulse surplus/minimum needed impulse) that a lizard of that size could generate. For instance, the vertical distance between the rightmost vertical arrows indicates that a 200 g lizard has the capacity to generate an 11 % impulse surplus (i.e. 111 % of what is needed to remain at the water surface). In contrast, the distance between the leftmost vertical arrows represents the prediction that a 2 g lizard has the capacity to generate a 125 % force surplus (225 % of the needed impulse). The upper dashed curve represents a prediction from a hydrodynamic model for the maximum slap-impulse contribution (maximum slap impulse/minimum needed impulse). The lower dashed curve was generated using a hydrodynamic model of the minimum slap-impulse contribution required for the lizard to avoid sinking into the water from one step to the next. The minimum slap-impulse contribution model is based on a prediction of the maximum possible stroke-impulse contribution (minimum slap impulse/needed impulse = 1 − maximum stroke impulse/needed impulse). The open circles are calculations of the slap-impulse contributions from individual steps. Three sequences in which lizards generated near-maximal slap-impulse contributions were identified (filled triangles). From these sequences, tracings were drawn of (B) 2.25 g, (C) 25.5 g and (D) 103.7 g lizards at the moment at which their feet reached their maximum depth below the water surface. These tracings demonstrate that, in spite of the fact that all three lizards are generating near-maximal slap-impulse contributions for their respective sizes, larger lizards must stroke more deeply into the water in order to generate the necessary stroke impulse to support their body weight. Tracings are not drawn to the same scale. Filled circles represent data from Glasheen and McMahon (1996*b*).

may help to explain why large lizards have a relatively low success rate when they attempt to run on water.

Our results also indicate that small lizards have the capacity to generate large force surpluses. In fact, we can estimate the maximum upward impulse that a lizard could generate if we assume that it could produce a maximal slap and a maximal stroke impulse in a single step (equations 3 and 4). A 2 g lizard has the capacity to generate an upward impulse that is more than twice (225 %) that needed to maintain its center of mass at a constant height. The 2 g lizard could, in theory, carry another 2 g lizard on its back as it runs across the water. A juvenile lizard can use this capacity to generate a force surplus to decelerate the center of mass when it drops onto the water surface from a branch overhanging the river. In contrast, large lizards cannot perform such feats because they can produce only small force surpluses. A 200 g lizard, under ideal conditions, can produce a force impulse that is just slightly greater than that needed to support its body weight (111 %). Because large lizards are able to produce only small force surpluses, they must avoid protraction drag by protracting their feet before the air cavity collapses. In contrast, small lizards, which are able to produce large force surpluses, do not always protract their feet before their short-lived cavities collapse (points below the curve, Fig. 8A).

Among the assumptions of the hydrodynamic model were that maximal values of f_{str}, u_{peak} and u_{rms} do not vary with body size, based on our measurements of the lizards' movements as they ran across the water surface. These assumptions are not entirely in agreement with predictions based on geometric scaling. In geometric scaling, the velocity of one body segment relative to another (u_{peak} and u_{rms}) would be expected to remain constant regardless of body size (Hill, 1950). However, f_{str} would be expected to vary with $M_b^{-0.33}$. If we were to use this scaling relationship for our estimates of the kinematic inputs to our model, it would not change any of our general conclusions; rather, it would only exaggerate the results presented in Fig. 9. Larger lizards would have an even smaller range of possible slap impulses, while small lizards would have a tremendous range of possible slap impulses.

A surprising finding was that the cavity drag and the timing of cavity collapse can be predicted simply on the basis of the measurement of the slap impulse and a knowledge of the relationships among these phenomena in experiments conducted with disks of various sizes (Glasheen and McMahon, 1996*a*). This suggests that the relationships among slap impulse, drag force and the timing of cavity collapse are rather robust and insensitive to changes in the shape of a flat plate (a circular disk *versus* a foot model; see Fig. 4). Therefore, future investigators in the area of low-speed water entry need only measure the slap impulse. Thereafter, drag forces and the timing of cavity collapse can be predicted using results for circular disks, as was done in Figs 6 and 7.

In summary, our finding that there is a physical basis underlying the size-dependent water-running ability of basilisk lizards lends credence to an ecological theory which suggests that a deteriorating water-running ability encourages larger basilisk lizards to move away from the river bank into a

different habitat (Laerm, 1974). The large lizard then tends to utilize resources found in its new habitat, rather than competing with small lizards along the river's edge. This partitioning of resources could result in reduced competition between young and adult lizards, thereby allowing higher overall population densities.

Appendix A

On a qualitative level, we evaluated the effect of surface tension by adding a small amount of detergent to the water tank in which the lizards ran. Detergent reduces the surface tension at the air–water interface to about half of its usual value (approximately $0.03\,N\,m^{-1}$ as opposed to $0.072\,N\,m^{-1}$) and therefore could reduce the lizards' ability to support their body weight on the water surface. However, we could not detect any change in performance due to a reduced surface tension. An analysis of the physics of water entry reveals why surface tension plays such a small role in the lizards' locomotion. To determine the maximal contribution of surface tension to the overall upward force, we calculated the ratio of surface tension force to inertial force for the conditions in which surface tension would play the largest role: the smallest lizard's foot ($r_{eff}\approx0.005\,m$) moving at the slowest speed ($u_{rms}\approx0.5\,m\,s^{-1}$). The upward force due to surface tension (D_γ) can be approximated as:

$$D_\gamma = 2\pi r_{eff}\gamma . \quad (A1)$$

The variable γ is the value for surface tension of pure water in air at 25 °C ($0.072\,N\,m^{-1}$). Excluding unsteady and gravitational effects, the upward force due to the fluid's inertia is:

$$D_{steady} = 0.5\, C_D^{*}\pi r_{eff}^2 \rho u_{rms}^2 , \quad (A2)$$

where C_D^{*} is the water-entry drag coefficient ($C_D^{*}\approx0.7$) and ρ is the density of water. Thus, the ratio between D_γ and D_{steady} is:

$$D_\gamma/D_{steady} = 5.7(\gamma/\rho r_{eff}u_{rms}^2) . \quad (A3)$$

Thus, if unsteady forces and hydrostatic pressure played no role in the lizards' locomotion, and the lizards were to support themselves using only dynamic pressure and surface tension, surface tension would still account for only 5 % of the overall support force.

Finally, while it is true that the perimeters of the lizards' feet are likely to be greater than $2\pi r_{eff}$, it is also evident that basilisks obtain a considerable support force from both unsteady forces and hydrostatic pressure.

Appendix B

To determine whether our simple model for the stroke impulse (equation 4) is appropriate, we calculated the model's prediction of the maximum contribution of the stroke impulse to the overall impulse needed. We compared the model's prediction for a 90 g lizard with detailed measurements from water-running observations on moderately sized lizards (approximately 90 g; Glasheen and McMahon, 1996*b*). We analyzed only the sequences in which the lizards stroked downwards into the water to their full leg length, to ensure that the detailed measurements were approximating maximum stroke efforts (12 sequences). The contribution from the stroke impulse to supporting body weight was calculated as follows:

$$\text{calculated stroke impulse/calculated needed impulse} = (C_D^{*}S\rho/M_b\boldsymbol{g}T_{step}) \int [0.5u^2(t) + \boldsymbol{g}h(t)]\cos\phi(t)\mathrm{d}t . \quad (B1)$$

The time-varying velocity of the mid-foot $u(t)$ was obtained by fitting a seventh-order polynomial to a plot of foot displacement *versus* time $h(t)$ and evaluating the derivative. Similarly, the angle of the normal of the foot relative to the vertical $\phi(t)$ was determined from a seventh-order polynomial fit of foot angle *versus* time. To calculate the stroke impulse, stroke force was integrated from the time when the lizard's foot first slapped the water surface until the time at which the mid-foot reached its greatest depth. We found that the results from our simple model (equation 4) agree rather well with the detailed calculations (equation B1); only a slight trend to overpredict the maximum stroke impulse contribution is evident (equation 4 / equation B1 = model stroke impulse contribution / detailed calculations of stroke impulse contribution = 1.06±0.10).

The authors would like to thank Marybel Soto of the Organization for Tropical Studies for her kind assistance in obtaining export permits for the lizards. Walter Meshaka provided crucial expertise in capturing and caring for the lizards. Assistance with data analysis was provided by Seth Wright. Finally, the support and advice of R. J. Full improved this manuscript in many ways. This study was supported by funds from the Office of Naval Research, the Putnam Expedition Committee, the Committee on Latin American and Iberian Studies (to J.W.G.) and the Systems Development Foundation (to T.A.M.).

References

BIRKHOFF, G. AND ZARANTONELLO, E. H. (1957). *Jets, Wakes and Cavities*. New York: Academic Press Inc.

GLASHEEN, J. W. AND MCMAHON, T. A. (1996*a*). Vertical water entry of disks at low Froude Numbers. *Physics of Fluids* **8**, 2078–2083.

GLASHEEN, J. W. AND MCMAHON, T. A. (1996*b*). A hydrodynamic model of locomotion in the Basilisk lizard. *Nature* **380**, 340–342.

HILL, A. V. (1950). The dimensions of animals and their muscular dynamics. *Sci. Prog.* **38**, 209–230.

LAERM, J. (1974). A functional analysis of morphological variation and differential niche utilization in basilisk lizards. *Ecology* **55**, 404–411.

RAND, A. S. AND MARX, H. (1967). Running speed of the lizard *Basiliscus basiliscus* on water. *Copeia* **1**, 230–233.

VAN DEVENDER, R. W. (1983). *Basiliscus basiliscus* (Chisbala, Garrobo, Basilisk, Jesus Christ Lizard). In *Costa Rican Natural History* (ed. D. H. Janzen), pp. 379–380. Chicago: University of Chicago Press.